Integration of Sentinel-1A and Sentinel-2B Data for Land Use and Land Cover Mapping of the Kirkuk Governorate, Iraq

Shareef, M. A.,[1]* Hassan, N. D.,[1] Hasan, S. F.[1] and Khenchaf, A.[2]
[1]Department of Surveying Engineering Techniques, Technical College of Kirkuk, Northern Technical University, Baghdad Road, 36001 Kirkuk, Iraq, E-mail: muntadher.a.shareef@ntu.edu.iq
[2]Lab-STICC UMR CNRS 6285, ENSTA Bretagne, 2 Rue François Verny, 29806 Brest Cedex 09, France
**Correspondance Author*

Abstract
Land use and land cover maps are essential to aid our knowledge of modelling the environment, managing water. Multispectral and SAR Satellite data consider the main and valuable resource for LULC mapping. Because of the presence of clouds, creating a precise LULC map using multispectral data is a challenge. Herein, the goal of this study is to generate a precise map of LULC of Kirkuk city using different classification methods and to evaluate the impact of combining SAR and optical Sentinel (1A and 2B) data on classification efficiencies. Gram–Schmidt (GS) method was applied to combine the multispectral Sentinel 2B data and Sentinel-1A (VH, VV). The efficiency of using four commonly-used classification algorithms was then compared to specify the optimal method for LULC classification. The finding reveals that the greatest accuracy of 97.93% with a kappa coefficient of 0.97 was produced using the SVM algorithm applied to multispectral Sentinel-2B data. while the DT-KNN algorithm was most efficient when it applied to Sentinel-2B-VH data with an accuracy of 97.60 %. The overall accuracy of RF is also improved when it applied to Sentinel-1A-VV than Sentinel-1A-VH and multispectral data. Additionally, the method developed will be helpful to researchers who continue to use diverse data sources to map various regions. These mapping results represent an essential step toward future soil mapping and mineral estimation.

1. Introduction

Human effectiveness produces a significant effect on the earth's surface. The land is used to provide needs of the physical aspects of Earth's surface, water distribution, urban areas and settlements, vegetation, soil, and additional physical characteristics including those generated by human effectiveness, and economic activities (Rawat and Kumar, 2015 and Shareef et al., 2016). Land-use and land-cover (LULC) have relied on determinants of natural, social, and economic activity and their use by human beings over time and in space. LULC maps are essential to support our knowledge of environmental modeling, water resource management (Riebsame et al., 1994), provide proper land management tools, and promote decision making (Yuan et al., 2005). Remote sensing is crucial standard technology for LULC mapping via diverse classification techniques over broad scales (Cihlar, 2000 and Kazemi et al., 2009). Optical satellite sensors confront the difficulty of obtaining information with the negligible existence of the cloud. The problem of acquiring proper cloud-free images from visual observation sensors has been studied previously (Hansen and Loveland, 2012 and Leinenkugel et al., 2014). Moreover, Synthetic Aperture Radar (SAR) is considering an active system that does not base on sunlight and can operate without being influenced by weather conditions or data obtaining duration, and has the potential to overcome the restraints of optical systems (da Costa Freitas et al., 2008).

Although the integration of multispectral bands and SAR data is promising for land application and LULC mapping, it remains rarely used (Joshi et al., 2016). Furthermore, numerous researches have confirmed the requirement for more efficient and improved mapping relies on the coupling of multispectral and SAR for classifications land (Forghani, 1994, Forghani et al., 2018, Joshi et al., 2016 and Waske and van der Linden, 2008). Moreover, the spatial resolution and revisit times have been improved with the lately Sentinel missions, leading to enhanced LULC mapping (Erinjery et al., 2018). Recent investigations have revealed data suitability of Sentinels-1A and multispectral Sentinel-2B for efficient mapping of various LULC classes. The high revisit of the Sentinel satellite is particularly encouraging.

The comparatively high-resolution data and wide

swath allow for suitable coverage on a large-scale with resolution of small-scale farmland (Steinhausen et al., 2018). The typical procedure for producing LULC map requires data classification, and examines diverse factors. The initial process of image classification usually depend upon determining an appropriate classification method (Lu and Weng, 2007). Choosing a proper algorithm of classification is crucial for obtaining precise LULC maps. Thus, various algorithms, approaches, and methodologies have applied for diverse applications and study areas (Elatawneh et al., 2014, Rawat and Kumar, 2015, Butt et al., 2015 and Shareef et al., 2016). Researchers have continually faced difficulties associated with determining which classification algorithm to use without any clear guidelines on choosing proper algorithms (Sameen et al., 2016). Herein, we evaluate the ability of SAR and multispectral Sentinel data for mapping LULC in the Kirkuk governorate, Iraq.

To assess the integrating possibility of data used, our principal goals are: (1) to confirm that an improve in the classification accuracy can be accomplished using different data sets, (2) to distinguish LULC feature through combining data used, (3) to test diverse classification methods to develop a classification procedure for LULC tailored to the region of interest.

2. Study Area

The area examined herein is Kirkuk governorate is situated in Northeast Iraq, with geographical coordinates of longitude 44° 00′ E and latitude 35° 13′ N. The chosen area covers 1,475.93 Km^2 as illustrated in Figure 1. LULC feature classes include urban, bare land, vegetation, various kinds of soils, water, and grassland (Mohammed Noori et al., 2018). Local steppe climate is the predominant climate in Kirkuk city, where there is limited rainfall throughout the year. The mean temperature and annual rains are about 21.6 °C and 365 mm respectively. The average precipitation is 0 mm in June, which is considered the driest month in the year while the most maximum rainfall is in March, with a mean of 73 mm. Kirkuk city situated between the northern mountainous of the study area and the flat areas of the south and south-west, as well as its abundant natural minerals and oil fields.

Various terrain and climate characteristics are present, which are representative of other areas of Iraq. The study area contains a combination of mountains, plateaus, valleys, and plains and all these geographical phenomena are characteristic of the climatic region, especially the temperature, rainfall, and wind. Also, the study region represents an area of high elevation in Iraq.

2.1 Satellite Data Description

Sentinel-1A SAR and Sentinel-2B images used for mapping the general LULC in the study area. Sentinel-1 instruments from the ESA-provided single and dual-polarized C-band SAR data with four acquisition modes. The interferometric wide (IW) swath was the primary mode for data obtaining overland with a 250 km swath at a ground resolution of 5 m by 20 m as a unique look. The Data collected was treated by the ESA into a geo-referenced image using ground range detected (GRD) products to provide continuous coverage of the area. Sentinel-2 was used in service on June 23, 2015, to supply more data as shown in Table 1. It contains 13 multispectral bands that can achieve a ground resolution of 10 to 60 m. The satellite bands range from 443 to 2190 nm, ensuring the capture of differences in the state of vegetation, including differences in vegetation type and temporal changes while reducing the variations in atmospheric photography (ESA, 2017).

The satellite data used in our study provided by the Copernicus Open Access Hub, which offers free, complete, and open access data for all Sentinel projects (ESA, 2017).

2.2 Reference Data

Reference data for a supervised classification were collected in December 2018, and divided into training and examining data to perform classification and classification accuracy. Evaluation data were produced using a GPS instrument as part of a field survey or by using high-resolution data (Lu et al., 2007). In this study, Google Earth and high-resolution satellite images were employed to generate reference (training and examining) data using version 5.3 by delineating the region of interest (ROIs) for every recognized feature on a high-resolution image of Kirkuk city. Subsequently, LULC was identified visually and separated into nine classes using the high-resolution images. During the sampling procedure, the examining data was chosen randomly for each classification type. The sampling positions were spread throughout the study area to achieve good classification results.

2.3 Data Preprocessing

Pre-processing was performed independently for Sentinel-1A SAR and multispectral Sentinel-2B data, as shown in Figure 2.

Table 1: SAR data used in the study

Satellite mission	Product type	Acquisition mode	Acquisition time	Bands	Resolution
Sentinel-1A	GRD	IW	7/11/2018	VV,VH	10 m
Sentinel-2B	GRD	MSI-L1C	29/10/2018	13 band	10–60 m

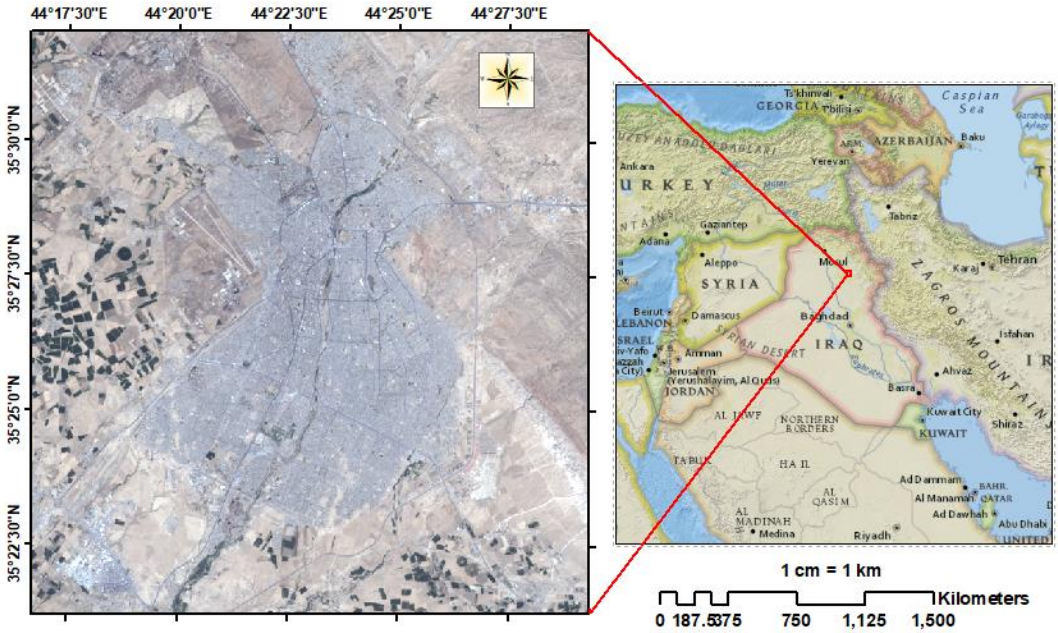

Figure 1: The study area

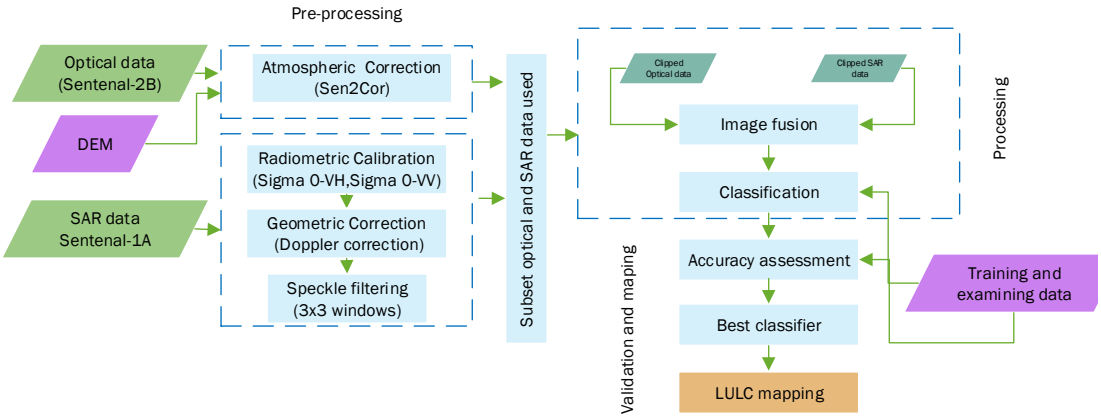

Figure 2: The general methodology of LULC mapping

Atmospheric correction using the Sen2Cor Sentinel-2 processor was used to transform a top-of-atmosphere (TOA) Level-1C into a bottom-of-atmosphere measurement (Müller et al., 2016). This accomplished terrain, atmospheric, and cirrus correction for the input data (Weiß, 2019). Radiometric correction of Sentinel-1 SAR models applied to polarizations of VH and VV of radar data were transformed into radar backscatter (sigma 0) using the methods developed by Miranda and Meadows (Miranda et al., 2015). The Doppler correction was applied to reduce geometric distortions occur in terrains based upon the digital elevation model (DEM) (Gascon et al., 2017) provided by SRTM with resolution of a 30 m. Noise effects in the radar images were reduced using a multi-temporal Lee filter with a 3 by 3-pixel window. The high-resolution worldview satellite image of Kirkuk city acquired in 2018 provided by Kirkuk governorate was also used in this study.

2.4 Image Fusion

Due to its popularity, the Gram-Schmidt (GS) fusion method was employed in this study, to merge the

multispectral Sentinel-2B images and Sentinel-1A, which has two polarizations (HV, VV). GS uses a non-orthogonal assemblage of independent roles and generates an orthogonal groundwork above an uncertain interval associated with the random weighting function (Amarsaikhan et al., 2012).

3. Methods

3.1 LULC Classification

Many classification algorithms were widely employed to describe as either supervised and unsupervised classification (Ban et al., 2010). To obtain the performance of the diverse classification techniques, we examined four algorithms (1) Random Forest (RF) (Breiman, 2001), (2) support vector machine (SVM) (Burges, 1998), (3) k-nearest neighbours (KNN) and The KD Tree KNN classifier (Altman, 1992). SVM separation data apply the highest division margins (Cortes and Vapnik, 1995). This algorithm used the Gaussian radial basis function (RBF) kernel and included two hyper-parameters to measure the resilience of the SVM: the regulation factor C and kernel bandwidth γ. High values of C reflect the higher penalties for integrated pixels. The γ value determines the range of training data, but no clear guidelines have provided regarding proper learning algorithms (Aizerman, 1964). RF is a set learning method that creates various trees rely on irregular bootstrapped examples in selected training samples (Breiman, 2001). This approach is robust against over-fitting and can manage many entering parameters without any removing of the variable. The outcomes specified by a maximum suggest of classification tree (Sonobe et al., 2017). KNN defines as a non-parametric computer learning process because it quickly identifies all its training data.

Notwithstanding its simplicity, KNN has applied for several classification challenges, including the analysis of various satellite data. KNN in the collection of training data affirms an assembly of K examples that are closest to the unknown patterns (based on a Euclidean distance function) (Weinberger and Saul, 2009). The KD Tree KNN classifier uses a KD Tree to improve performance but should give the same result as the slow KNN classifier (Ng and Lippmann, 1991). A KD tree is described as space-partitioning for data structuring and creating points in k-dimensional space. The k-d trees are a suitable data structure for various applications, including searches that involve a multidimensional exploration key (e.g., nearest neighbor or range searches) (Weinberger and Saul, 2009).

3.2 Accuracy Assessment

The confusion matrix is employed to assess the accuracy of the classifier. It is a representative number of classified and reference data. It is a square configuration of n x n dimensions where n is the class number under consideration. Commonly used classification accuracies include the overall, user's, and producer's accuracies, as well as coefficient of kappa (Foody, 2002). The importance of the specialized knowledge of the kappa coefficient is equivalent to the overall accuracy (OA) in the confusion matrix. Furthermore, the overall accuracy provides the likelihood of (Pontius Jr and Millones, 2011 and Olofsson et al., 2013) correctness in the classified image. The producer's accuracy is defined by the rate of the correctly classified pixel, while the user's accuracy in the error matrix can be determined as the rate of pixels that correctly classified of the class and whole number of pixels classified by the classifier for that class.

4. Results

4.1 Classification of Multispectral Sentinel Data

In the first analysis, a confusion matrix was employed to assess the classification outcomes of methods implemented for the multispectral Sentinel-2B data. The mechanism of the different classifiers was examined to define the performance of each classifier relative to the data used. Figure 3 illustrates the finding of the LULC classification analysis performed using ENVI version 5.3. Post-classification executed using three methods: sieve, minority, and clump analysis. Sieve class analysis was used to resolve the issues of single pixels in classified images as it removes isolated labeled pixels using blob grouping. The majority analysis was used to regulate false pixels inside a particularly important group to the proper pixel group. Clump analysis was used to compile adjacent similarly classified regions together by applying morphological operators. Visually, the classifiers exhibited intimate behavior for organizing the multispectral Sentinel-2B data via simple differences.

SVM provided an excellent outcome in both visual and statistical interpretation, with an OA of 97.93%. No essential distinctions were recognized between the KNN and RF algorithms, showing a negligible difference of 0.43%. However, the sequences showed that the classification accuracy was improved using DT-KNN with an OA value of 94.83% compared to using the KNN and RF algorithms as illustrated in Table 2.

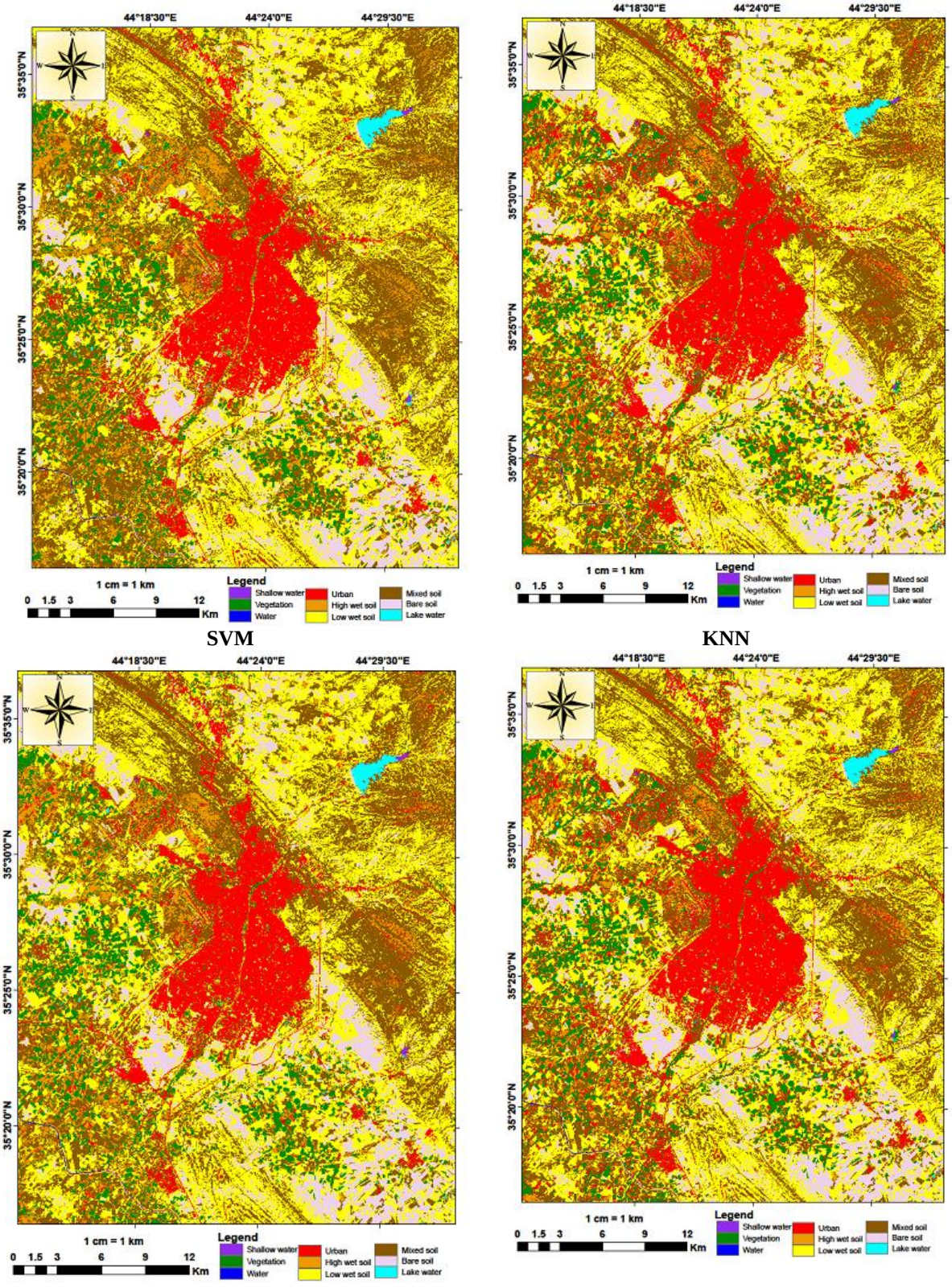

Figure 3: Different classifiers applied to the Sentinel-2B data with post-classification methods

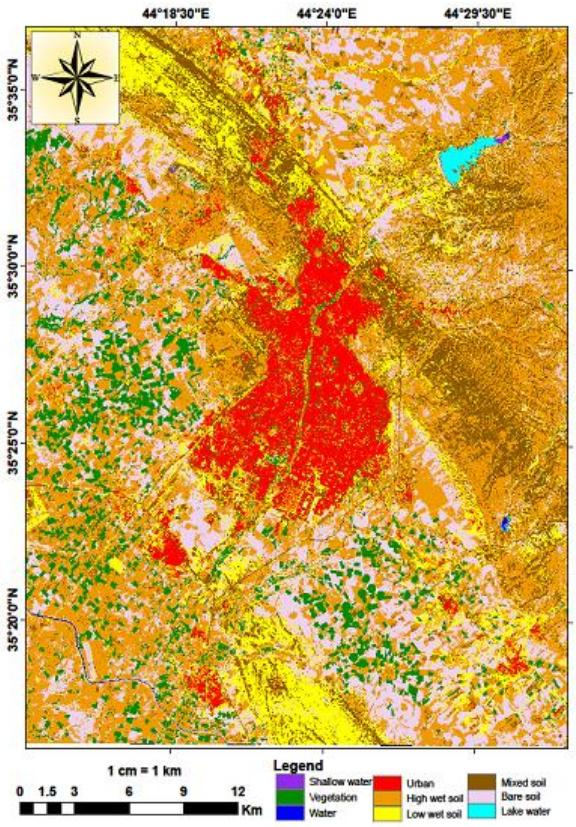

Original SVM (VH)

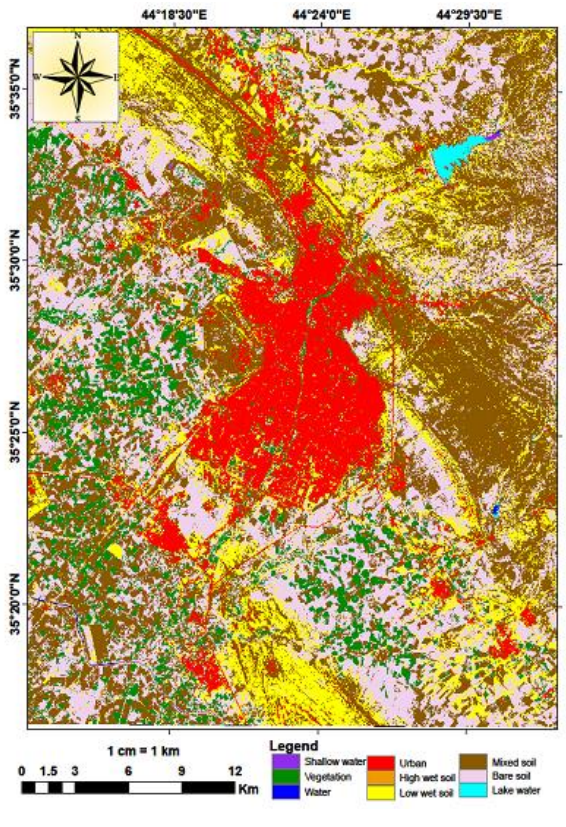

KNN (VH)

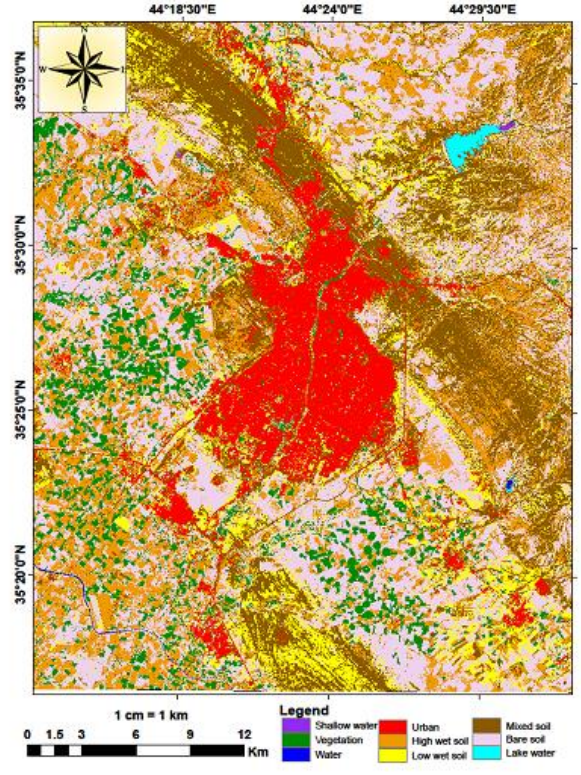

DT-KNN (VH)

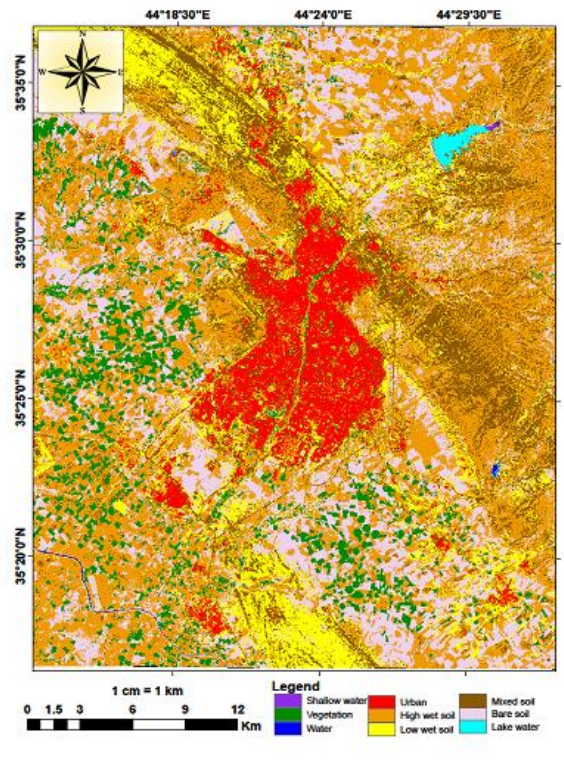

RF (VH)

Figure 4: Post-classification of the fused VH and VV images (continune next page)

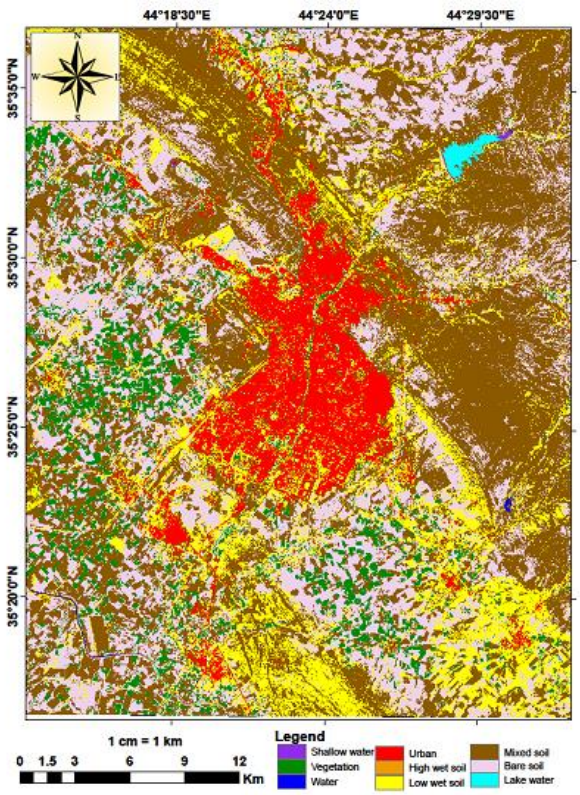

SVM (VV)

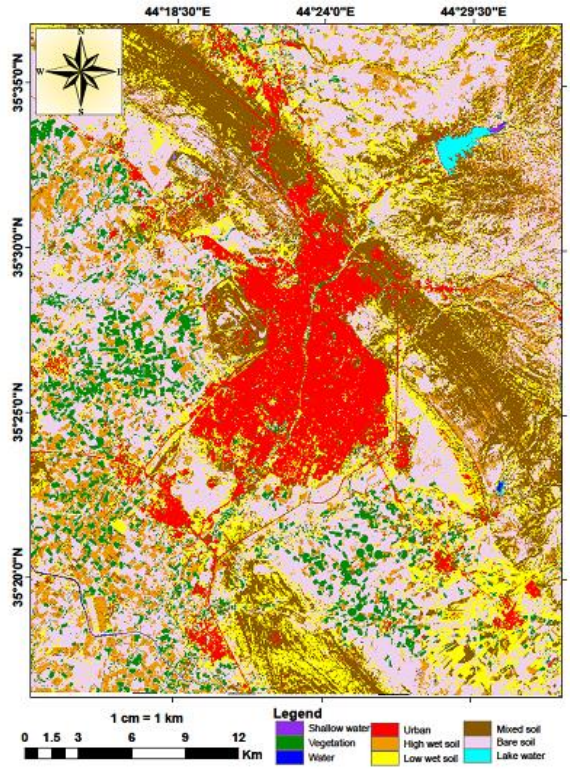

KNN (VV)

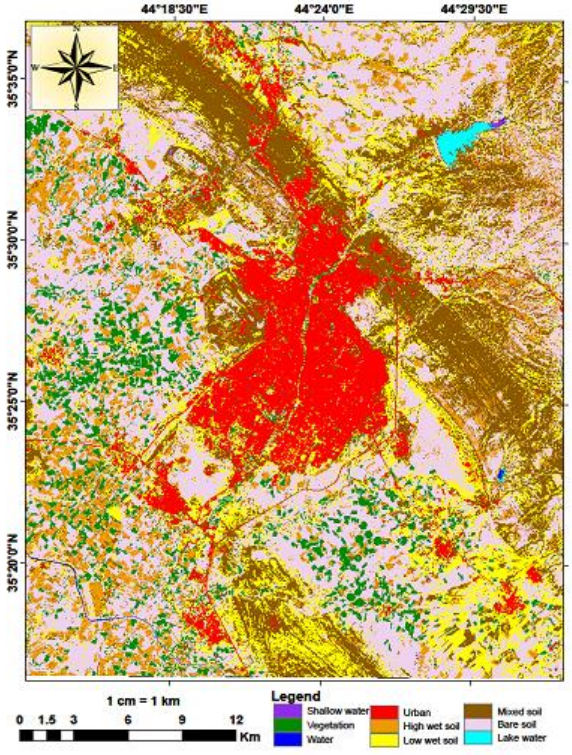

DT-KNN(VV)

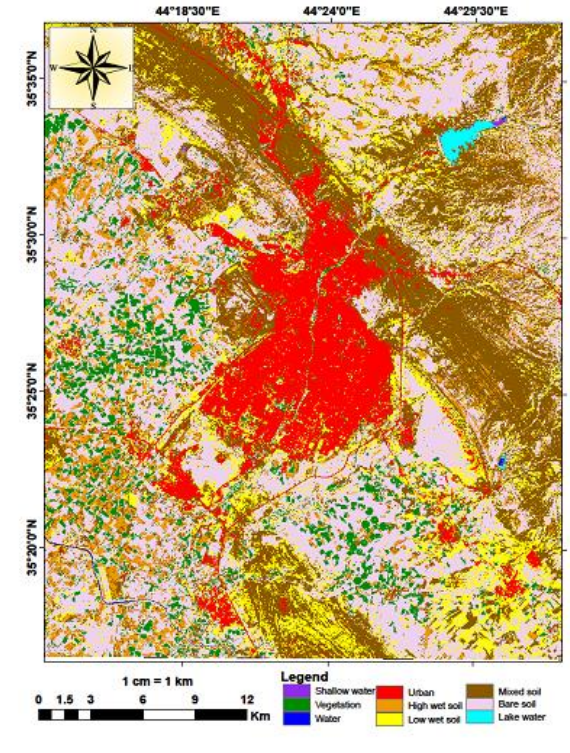

RF(VV)

Figure 4: Post-classification of the fused VH and VV images

Table 2: Overall Accuracy and Kappa coefficient of the various classifiers

Data set	Classifier	Overall Accuracy (%)	Kappa coefficient (K)
Sentinel-2B	DT-KNN	94.8276	0.9398
	KNN	93.5345	0.9251
	RF	93.9655	0.9295
	SVM	97.9339	0.9760
Sentinel-1A-VH	DT-KNN	97.6096	0.9722
	KNN	86.8526	0.8481
	RF	92.5743	0.9122
	SVM	93.2271	0.9214
Sentinel-1A-VV	DT-KNN	97.2112	0.9676
	KNN	97.2112	0.9676
	RF	94.8207	0.9399
	SVM	84.8606	0.8252

4.2 Classification of Combined Sentinel (1A and 2B) Data

The essential goal of this analysis was performed to assess the use of Sentinel-1A data in developing LULC assignment accuracy. The consequent experiment evaluated the integration of Sentinel-1A data featuring different polarization (HV, VV) with multispectral sentinel-2B data to refine the performance for increasing the accuracy of LULC classification. The GS fusion method was applied twice; once to fuse the multispectral Sentinel-2B (R, G, B, IR) data with Sentinel-1A (VH) data to produce the Sentinel-2B-VH image, and additionally to merge Sentinel-2B (R, G, B, IR) data with Sentinel-1A (VV) data to create the Sentinel-2B-VV image (Figure 4). However, the same classifier employed in the first analysis was implemented for the combined Sentinel-2B-VH and Sentinel-2B-VV image data. Three post-classification methods (sieve, minority, and clump) were also applied. Visually, high wet soil was demonstrated using the SVM algorithm on the Sentinel -2B-VH image with the apparent absence of vegetation and wet soil. Mixed soil was shown with good separation between the vegetation, and bare soil was best separated using the KNN algorithm. RF reflects a majority of the bare soil distribution relative to the water body classes, including lake and river water (Figure 4). Classification of the Sentinel-2B-VV image revealed a different classifier behavior. The mixed and wet soils were demonstrated in almost all classified images. Most residential and urban areas were classified as wetlands, and some agricultural fields were classified as wetlands or mixed soil areas. The KNN classifier showed a clear superiority of open soil areas with no water areas (rivers or small lakes). This analysis was compared to the finding of applying only multispectral Sentinel-2B data to assess the efficiency of the Sentinel-1A SAR data in LULC mapping. The data presented in Table 2 confirms that when Sentinel-1A data were fused with multispectral Sentinel-2B images, OA improved with most of the applied classifiers. The OA was augmented with DT-KNN for Sentinel-2B-VH and increased for the DT-KNN, KNN and RF algorithms used on the Sentinel-2B-VV images, as illustrated in Table 2. otherwise, this combination reduced the classification accuracy when the KNN, RF, and SVM algorithms were used, achieving OA values of 86.85%, 92.57%, and 93.2271%, respectively. This demonstrates that Sentinel-1A enhanced the performance of LULC classification depends on the polarization used as a method of classification.

5. Discussion

A comparison table was generated relied upon n the two analyses f the Sentinel data. Table 2 shows the OA and kappa coefficient calculated for each of the classifiers applied. The greatest OA (97.93%) was achieved using the SVM algorithm applied to multispectral Sentinel-2B data with a kappa coefficient of 0.97. The DT-KNN algorithm was determined to operate most efficiently when applied to the Sentinel-2B-VH fused via the GS algorithm with an OA equal to 97.60% and a kappa of 0.97. The results showed that DT-KNN yielded the highest accuracy through the use of the original Sentinel-1A SAR or by using the enhanced Lee-filtered SAR data were combined with the Sentinel-2B images. Generally, DT-KNN accomplished exceptionally well with most data utilized in process of the classification and exhibited improved accuracy. The KNN accuracy improved when Sentinel-A1(VV) was used, but DT-KNN and KNN algorithms showed similar or better results using Sentinel-1A-VV with an OA of 97.2112% and a kappa coefficient of 0.96. The finding reveals that the SAR data increases the accuracy of LULC classification, where the preponderance of the most exceptional accuracies was noted when the SAR data were combined with multispectral sentinel data.

6. Conclusion

The integration of Sentinel-1A and Sentinel-2B data

for producing the LULC map through the classification of the Kirkuk governorate was examined herein. The classification efficiency was considerably improved by combing the SAR and multispectral data of the various satellites. It is essential to emphasize that only using the SAR image improved the LULC map in terms of precision, while the accuracy was further enhanced by adding supplementary scenes. In spite of the fact the multi-imagery method improved the efficiencies of classification, some LULC types were enhanced by fusing radar and optical data, mainly when DT-KNN was applied for almost all classifications used herein. Depending on outcomes, many approaches for more stable LULC mapping in diverse area was presented. The proposed methodology herein could be duplicated for similar areas of interest. Hence, associated companies and government establishments could benefit from using the outcomes. Further studies will include analysis of the spectral distinction potential of the Sentinel-1 and Sentinel -2 data for mapping of various kinds of vegetation and soils. Therefore, this study strongly recommends SAR and optical images integration for LULC mapping in diverse areas.

References

Aizerman, M. A., 1964, Theoretical Foundations of the Potential Function Method in Pattern Recognition Learning. *Automation And Remote Control*, Vol. 25, 821-837.

Altman, N. S., 1992, An Introduction to Kernel and Nearest-Neighbor Nonparametric Regression. *The American Statistician*, Vol. 46, 175-185.

Amarsaikhan, D., Saandar, M., Ganzorig, M., Blotevogel, H., Egshiglen, E., Gantuyal, R., Nergui, B. and Enkhjargal, D., 2012, Comparison of Multisource Image Fusion Methods and Land Cover Classification. *International Journal of Remote Sensing*, Vol. 33, 2532-2550.

Ban, Y., Hu, H. and Rangel, I. M., 2010, Fusion of Quickbird MS and Radarsat SAR Data for Urban Land-Cover Mapping: Object-Based and Knowledge-Based Approach. *International Journal of Remote Sensing*, Vol. 31, 1391-1410.

Breiman, L., 2001, Random Forests. *Machine Learning*, Vol. 45, 5-32.

Burges, C. J., 1998, A Tutorial on Support Vector Machines for Pattern Recognition. *Data Mining And Knowledge Discovery*, Vol. 2, 121-167.

Butt, A., Shabbir, R., Ahmad, S. S. and Aziz, N., 2015, Land Use Change Mapping and Analysis Using Remote Sensing and GIS: A Case Study of Simly Watershed, Islamabad, Pakistan. *The Egyptian Journal of Remote Sensing and Space Science*, Vol. 18, 251-259.

Cihlar, J., 2000., Land Cover Mapping of Large Areas from Satellites: Status and Research Priorities. *International Journal of Remote Sensing*, Vol. 21, 1093-1114.

Cortes, C. and Vapnik, V., 1995, Support-Vector Networks. *Machine Learning*, Vol. 20, 273-297.

Da Costa Freitas, C., De Souza Soler, L., Sant'anna, S. J. S., Dutra, L. V., Dos Santos, J. R., Mura, J. C. and Correia, A. H., 2008, *Land Use and Land Cover Mapping in the Brazilian Amazon Using Polarimetric Airborne P-Band SAR Data. Ieee Transactions on Geoscience and Remote Sensing*, Vol. 46, 2956-2970.

Elatawneh, A., Kalaitzidis, C., Petropoulos, G. P. and Schneider, T., 2014, Evaluation of Diverse Classification Approaches for Land Use/Cover Mapping in a Mediterranean Region Utilizing Hyperion Data. *International Journal of Digital Earth*, Vol. 7, 194-216.

Erinjery, J. J., Singh, M. and Kent, R., 2018, Mapping and Assessment of Vegetation Types in the Tropical Rainforests of the Western Ghats Using Multispectral Sentinel-2 and SAR Sentinel-1 Satellite Imagery. *Remote Sensing of Environment*, Vol. 216, 345-354.

ESA, 2017, 2sentinels Scientific Data Hub. Retrieved From. https://scihub.copernicus.eu/-dhus/#/home.

Foody, G. M., 2002, Status of Land Cover Classification Accuracy Assessment. *Remote Sensing of Environment*, Vol. 80, 185-201.

Forghani, A., 1994, A New Technique for Map Revision and Change Detection Using Merged Landsat TM and Spot Sets in a Urban Environment. *Asian-Pasific Remote Sensing J.*, Vol. 7, 119-129.

Forghani, A., Nadimpalli, K. and Cechet, R. P., 2018, Extracting Terrain Categories from Multi-Source Satellite Imagery. *International Journal of Geoinformatics*, Vol. 14, 25-34.

Gascon, F., Bouzinac, C., Thépaut, O., Jung, M., Francesconi, B., Louis, J., Lonjou, V., Lafrance, B., Massera, S. and Gaudel-Vacaresse, A., 2017, Copernicus Sentinel-2a Calibration and Products Validation Status. *Remote Sensing*, Vol. 9, 584.

Hansen, M. C. and Loveland, T. R., 2012, A Review of Large Area Monitoring of Land Cover Change Using Landsat Data. *Remote Sensing of Environment*, Vol. 122, 66-74.

Joshi, N., Baumann, M., Ehammer, A., Fensholt, R., Grogan, K., Hostert, P., Jepsen, M., Kuemmerle, T., Meyfroidt, P. and Mitchard, E., 2016, A Review of the Application of Optical and Radar Remote Sensing Data Fusion to Land Use Mapping and Monitoring. *Remote Sensing*, Vol.

8, 70.

Kazemi, S., Lim, S. and Rizos, C., 2009, Interactive and Automated Segmentation and Generalisation of Raster Data. *International Journal of Geoinformatics*, Vol. 5(3), 1-11.

Leinenkugel, P., Wolters, M. L., Kuenzer, C., Oppelt, N. and Dech, S., 2014, Sensitivity Analysis for Predicting Continuous Fields of Tree-Cover and Fractional Land-Cover Distributions in Cloud-Prone Areas. *International Journal of Remote Sensing*, Vol. 35, 2799-2821.

Lu, D. and Weng, Q., 2007, A Survey of Image Classification Methods and Techniques for Improving Classification Performance. *International Journal of Remote Sensing*, Vol. 28, 823-870.

Miranda, N., Meadows, P., Type, D. and Note, T., 2015, Radiometric Calibration of S-1 Level-1 Products Generated by the S-1 IPF. viewed at Https://Sentinel. Esa. Int/Documents/247904/685163/S1-Radiometric-Calibration-V1. 0. Pdf.

Mohammed Noori, A., Falih Hasan, S., Mahmood Ajaj, Q., Ridha Mezaal, M., Z. M. Shafri, H. and Aidi Shareef, M., 2018, *Fusion of Airborne Hyperspectral and Worldview2 Multispectral Images for Detailed Urban Land Cover Classification a Case Study of Kuala Lumpur*, Malaysia. 2018, 7, 5.

Müller, H., Griffiths, P. and Hostert, P., 2016, Long-Term Deforestation Dynamics in the Brazilian Amazon-Uncovering Historic Frontier Development along the Cuiabá–Santarém Highway. *International Journal of Applied Earth Observation and Geoinformation*, Vol. 44, 61-69.

Ng, K. and Lippmann, R. P. A., 1991, Comparative Study of the Practical Characteristics of Neural Network and Conventional Pattern Classifiers. Advances in Neural Information Processing Systems, 970-976.

Olofsson, P., Foody, G. M., Stehman, S. V. and Woodcock, C. E., 2013, Making Better Use of Accuracy Data in Land Change Studies: Estimating Accuracy and Area and Quantifying Uncertainty Using Stratified Estimation. *Remote Sensing of Environment*, Vol. 129, 122-131.

Pontius Jr, R. G. and Millones, M., 2011, Death to Kappa: Birth of Quantity Disagreement and Allocation Disagreement for Accuracy Assessment. *International Journal of Remote Sensing*, Vol. 32, 4407-4429.

Rawat, J. and Kumar, M., 2015, Monitoring Land Use/Cover Change Using Remote Sensing and GIS Techniques: A Case Study of Hawalbagh Block, District Almora, Uttarakhand, India. *The Egyptian Journal of Remote Sensing and Space Science*, Vol. 18, 77-84.

Riebsame, W. E., Meyer, W. B. and Turner, B., 1994, Modeling Land Use and Cover as Part of Global Environmental Change. *Climatic Change*, Vol. 28, 45-64.

Sameen, M. I., Nahhas, F. H., Buraihi, F. H., Pradhan, B. and Shariff, A. R. B. M., 2016, A Refined Classification Approach by Integrating Landsat Operational Land Imager (OLI) and Radarsat-2 Imagery for Land-Use and Land-Cover Mapping in a Tropical Area. *International Journal of Remote Sensing*, Vol. 37, 2358-2375.

Shareef, M. A., Khenchaf, A. and Toumi, A., 2016, Integration of Passive and Active Microwave Remote Sensing to Estimate Water Quality Parameters. Ieee Radar Conference (Radarconf), IEEE, 1-4.

Sonobe, R., Tani, H. and Wang, X., 2017, An Experimental Comparison Between Kelm and Cart for Crop Classification Using Landsat-8 OLI Data. *Geocarto International*, Vol. 32, 128-138.

Steinhausen, M. J., Wagner, P. D., Narasimhan, B. and Waske, B., 2018, Combining Sentinel-1 and Sentinel-2 Data for Improved Land Use and Land Cover Mapping of Monsoon Regions. *International Journal of Applied Earth Observation and Geoinformation*, Vol. 73, 595-604.

Waske, B. and Van Der Linden, S., 2008, Classifying Multilevel Imagery from SAR and Optical Sensors by Decision Fusion. IEEE Transactions on Geoscience and Remote Sensing, Vol. 46, 1457-1466.

Weinberger, K. Q. and Saul, L. K., 2009, Distance Metric Learning for Large Margin Nearest Neighbor Classification. *Journal of Machine Learning Research*, Vol. 10, 207-244.

Weiß, T., 2019, *Multiply Sar Pre-Processing Documentation*. https://buildmedia.readthedocs.org/media/pdf/multiply-sar-pre-processing/latest/multiply-sar-pre-processing.pdf

Yuan, F., Sawaya, K. E., Loeffelholz, B. C. and Bauer, M. E., 2005, Land Cover Classification and Change Analysis of the Twin Cities (Minnesota) Metropolitan Area by Multitemporal Landsat Remote Sensing. *Remote Sensing of Environment*, Vol. 98, 317-328.